Waves in Random and Complex Media
Vol. xx, No. x, xxxx 2006, 1–12

Taylor & Francis
Taylor & Francis

Bistatic scattering from an anisotropic sea surface: Numerical comparison between the first-order SSA and the TSM models

A. AWADA*, M. Y. AYARI, A. KHENCHAF and A. COATANHAY*

ENSIETA/E^3I^2 Laboratory-EA3876, 2 rue Francois Verny, Brest 29806 cedex 09, France

(Received ; revised ; in final form) Q1

The first-order small-slope approximation (SSA-1) model is used for numerical predictions of the normalized radar cross section (NRCS) of an anisotropic ocean surface in bistatic configurations for the K_u-band radar frequency. The calculations were made by assuming the Elfouhaily *et al.* surface-height spectrum for fully developed seas. In the forward–backward case, the SSA-1 presents an agreement with the geometric optics limit of the Kirchhoff approximation results in the near-specular directions where it is well known that the last model works well. In the fully bistatic case, SSA-1 numerical results are compared with those of the two-scale model in several configurations as a function of wind speed, wind direction, incident/scattering angles and for co- and cross-polarization states. Good agreement between the two models is noted in the co- and cross-polarization case with a small difference of about 1–2 dB. But in certain configurations, the SSA-1 model tends to overestimate the radar cross section peak behaviour. This irregularity is discussed and interpreted. *The main purpose of this paper is to analyse NRCS predictions based on the SSA-1 model in a fully bistatic configuration.*

Keywords: Bistatic scattering; Radar cross section; Small slope approximation

1. Introduction

Bistatic systems offer certain advantages of spatial diversity and some level of covertness not offered by monostatic systems. Recently bistatic and multistatic radar systems operating from air-borne and space-borne platforms acquired a renewed interest for its advantages in remote sensing of ocean surfaces [1, 2].

These applications require the development of accurate models to predict the radar bistatic scattering from such surfaces. Approximate models are still a necessity owing to the insurmountable numerical complexity of realistic scattering problems [3]. The most popular approximations in this context are the small perturbation model (SPM) [4] and Kirchhoff approximation (KA) [5]. Owing to its simplicity in the bistatic configuration, the geometric optics limit of the Kirchhoff approximation (KA-GO) is widely used for modelling quasi-specular forward scattering. However, in some cases this approach could be insufficient [6]. The KA-GO works well in the near-specular directions but gives inaccurate results in directions far from specular, where the Bragg mechanism produces scattering of the same order of magnitude. Unlike the KA and the SPM, the two-scale model (TSM, composite model) was

*Corresponding author. E-mail: awadaah@ensieta.fr, arnaud.coatanhay@ensieta.fr

Waves in Random and Complex Media
ISSN: 1745-5030 (print), 1745-5049 (online)
http://www.tandf.co.uk/journals
DOI: 10.1080/17455030600844089

suggested [7] for treating the scattering problem from surfaces with two roughness scales. This model was applied to the sea surface scattering problem in the monostatic case [8] and in the bistatic case [9]. However, this model introduces a scale-dividing parameter K_d separating small- and large-scale components of the roughness that can be arbitrary chosen within wide limits [10]. The advantage of this model is that it is easily applied. The predictions depend on how the surface is partitioned, and, together with difficulty in establishing the accuracy of the theory, these are the two drawbacks of this model [11]. Recently, Voronovich developed the small-slope approximation (SSA) [12, 13], which overcame the above mentioned drawbacks. It does not invoke any arbitrary parameters. For the Gaussian statistics of roughness, the result can be expressed strictly in terms of a rough spectrum. The SSA can be applied to an arbitrary wavelength, provided the tangent of grazing angles of incident/scattered radiation sufficiently exceeds RMS slopes of roughness [10]. This method has been widely tested, discussed and compared with other approximations by many authors in the monostatic case (backscattering) [10, 11, 14–16]. However, even if some works have been published in the forward scattered case [6, 17–19] no thorough study has yet been presented using the SSA in the fully bistatic case. This is the object of this paper. We will focus on presenting numerical results to analyse the potential applications of this model. It must be noted that, more recently, Elfouhaily *et al.* [20] developed a new unifying theoretical model called the weighted curvature approximation (WCA). This model was tested [21] in some particular bistatic configurations for Gaussian random surfaces were a good results are obtained.

In Section 2, some theoretical principles and the derivation of the SSA are briefly reviewed. Modelling the sea surface-height spectrum is required in order to solve the scattering problem; therefore, in Section 3, we describe the appropriate Elfouhaily [22] spectrum model. Section 4 will be dedicated to numerical results in the bistatic configuration that are analysed as a function of different parameters: wind speed, wind direction and scattering angles for the co- and cross-polarization cases. Some concluding remarks are presented in the final section.

2. Scattering cross section in the small slope approximation

SSA was proposed by Voronovich [12, 13] as a unifying theory that could reconcile SPM and KA without introducing the roughness scale division parameter K_d. It is an analytical approach, appropriate for scattering from both large- (high-frequency regime), intermediate- and small-scale (low-frequency regime) roughness scales within a single theoretical scheme. Thus it encompasses both Bragg and Kirchhoff mechanisms of scattering. In contrast to classical theories, the SSA is applicable irrespective of the wavelength of radiation, provided the tangent of grazing angles of incident/scattered radiation sufficiently exceeds the RMS slopes of roughness.

In this section, we present a brief summary of the analytical principles of this model. In our study, we consider a three-dimensional (3-D) problem of electromagnetic wave scattering by a 2-D rough sea surface, which is described as a random height function $h(\boldsymbol{r})$, where $\boldsymbol{r} = (x, y)$ is the vector position on the plane.

The geometrical configuration adopted for solving the wave-scattering problem is given in figure 1.

The small-slope approximation (SSA) presents an explicit expression for the scattering amplitude (SA) $S(\boldsymbol{k}, \boldsymbol{k}_0)$ on the basis plane waves in terms of parameters of the incident and scattered waves and surface roughness elevations $h(\boldsymbol{r})$ [13]. Both the lowest-order approximation (denoted SSA-1) and the next-order approximation (referred to as SSA-2), which is a correction of the lowest-order one, can be calculated. For higher orders, the derivation

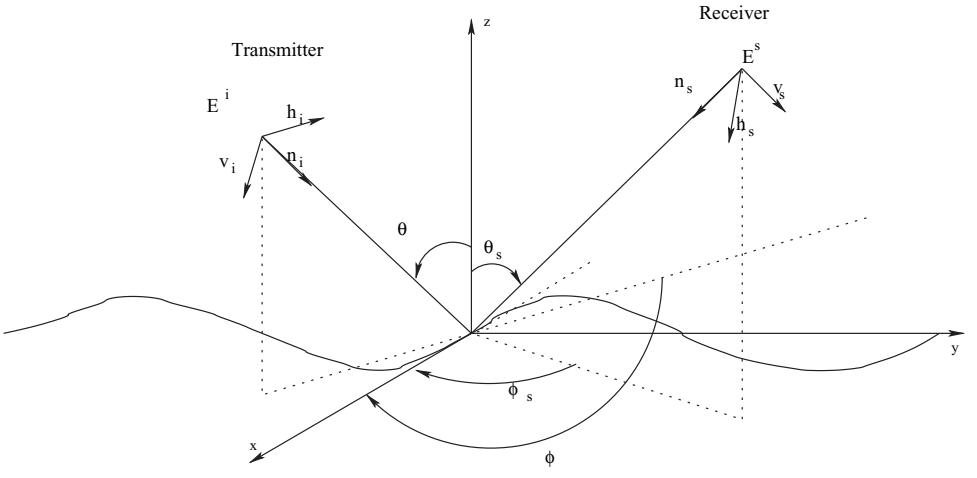

Figure 1. Geometrical configuration for wave-scattering from the sea surface.

becomes too involved. At the first order, the scattering amplitude has the following expression [10]:

$$S(\boldsymbol{k},\boldsymbol{k}_0)=\frac{2(q_kq_0)^{1/2}}{q_k+q_0}\mathrm{B}(\boldsymbol{k},\boldsymbol{k}_0)\int\frac{\mathrm{d}\boldsymbol{r}}{(2\pi)^2}\exp\left[-\mathrm{i}(\boldsymbol{k}-\boldsymbol{k}_0)\cdot\boldsymbol{r}+\mathrm{i}(q_k+q_0)h(\boldsymbol{r})\right]. \tag{1}$$

In equation (1), $\boldsymbol{k}_0$ and $\boldsymbol{k}$ are horizontal projections of the wavevector of incident and scattered waves, correspondingly, and $h(\boldsymbol{r})$ is the surface roughness elevation. Values $-q_0$ and q_k are appropriate vertical projections of the wavevectors defined as

$$q_0=\sqrt{\frac{w^2}{c^2}-k_0^2}\qquad q_k=\sqrt{\frac{w^2}{c^2}-k^2}\qquad \mathrm{Im}\,q_0,q_k\geq 0. \tag{2}$$

Here B is the first-order kernels of SPM. It is a 2×2 matrix. Assuming a statistically Gaussian sea surface, for a far field and a negligible coherently scattered field, the expression for the normalized bistatic cross-section (NBCS) with the first-order SSA model used in our numerical calculations is expressed as follows [10]:

$$\begin{aligned}\sigma_{\alpha\alpha_0}(\boldsymbol{k},\boldsymbol{k}_0)=\frac{1}{\pi}\left|\frac{2q_k\,q_0}{q_k+q_0}B_{\alpha\alpha_0}(\boldsymbol{k},\boldsymbol{k}_0)\right|^2\times\exp\left[-(q_k+q_0)^2C\,(0)\right]\\ \times\int\left\{\exp[(q_k+q_0)^2C(\boldsymbol{r})]-1\right\}\exp\left[-\mathrm{i}(\boldsymbol{k}-\boldsymbol{k}_0)\cdot\boldsymbol{r}\right]\mathrm{d}\boldsymbol{r},\end{aligned} \tag{3}$$

where $B_{\alpha\alpha_0}(\boldsymbol{k},\boldsymbol{k}_0)$ is a non-singular dimensionless function depending on polarization. Explicit expressions for it can be found in reference [13]. α,α_0 correspond to the polarization of scattered and incident plane waves, respectively. To evaluate the small-slope approximation and obtain the scattering cross sections, the correlation function $C(\boldsymbol{r})$ of the rough surface $h(\boldsymbol{r})$ is required:

$$C(\boldsymbol{r})=\int_0^{2\pi}\mathrm{d}\psi\int_0^{\infty}\mathrm{W}(\boldsymbol{K})\exp\left(\mathrm{i}\boldsymbol{K}\cdot\boldsymbol{r}\right), \tag{4}$$

where $\mathrm{W}(\boldsymbol{K})$ is the directional wavenumber spectrum of the rough surface, and ψ is the azimuthal angle measured with respect to the mean wind direction. In numerical computations, the correlation function $C(\boldsymbol{r})$ should be evaluated at a large number of points $\boldsymbol{r}$ throughout the

area of integration in equation (3). As will be shown later in equation (7), the evaluation of the correlation function can be considerably simplified. Many publications [10, 11, 16] show that for radar microwave backscattering (monostatic case) and for the range of scattering angles of interest for remote sensing, SSA-1 can be used with a mean accuracy of about 1 dB.

Following that conclusion, we have decided to accept a small margin of error in our bistatic numerical results by applying the SSA-1 in order to simplify the computation.

3. Sea spectrum: Elfouhaily model

Computing of the bistatic scattering cross section requires knowledge of either the sea spectrum or the sea surface height autocorrelation function, which is obtained from the Fourier transform of the sea spectrum. These representations must answer to the ergodicity and stationarity properties. The Pierson spectrum [23] is one of the first spectra published in the literature to describe capillary and gravity waves. The gravity region has been modified by adding the JONSWAP behaviour [24], in which the fetch effect is accounted for. Thus, we can also quote the Apel spectrum [25], which is a synthesis of work done in the 80s and 90s. Unfortunately, as shown by Elfouhaily *et al.* [22], this spectrum does not agree with the slope model proposed by Cox and Munk. This discrepancy is due to an inaccuracy in the description of the capillary waves.

In our simulations, we used the Elfouhaily model for the sea roughness spectrum (unified spectrum), which was recently developed based on available field and wave-tank measurements, and which is backed up by strong physical arguments—contrary to other spectra that are mostly empirical. It is important to note that this model was developed without any relation to remote-sensing data. Its agreement with the slope model proposed by Cox and Munk and with actual remote sensing data make it a credible model.

In general, the directional wave spectrum $\mathrm{W}(\boldsymbol{K})$ in equation (4) is the product of the non-directional spectrum $\mathrm{W}(K)$ with a spreading function $\mathrm{G}(\boldsymbol{K})$.

In polar coordinates, the general form of the Elfouhaily spectrum is as follows:

$$\mathrm{W}(\boldsymbol{K}) = \mathrm{W}(K, \psi) = \mathrm{W}(K)\mathrm{G}(K, \psi) \tag{5}$$

$$\mathrm{W}(K) = (B_{\mathrm{L}} + B_{\mathrm{H}})/K^3 \qquad \text{and} \qquad \mathrm{G}(\boldsymbol{K}) = [1 + \Delta(K)\cos(2\psi)]/2\pi, \tag{6}$$

where B_{L} and B_{H} are the respective contributions from low (gravity waves) and high (capillary waves) wavenumbers. $\mathrm{G}(K, \psi)$ is normalized such that $\int_0^\infty \mathrm{G}(K, \psi)\,\mathrm{d}\psi = 1$.

The calculation of the sea height correlation function in equation (4) based on the Elfouhaily spectrum possess a simplified analytical solution. With the help of Bessel functions, it reduces to two 1-D integrals over K [26]:

$$C(\boldsymbol{r}) = C(r, \phi) = C_0(r) - \cos(2\phi) \times C_2(r) \tag{7}$$

$$C_0(r) = \int_0^\infty S(K)J_0(Kr)\mathrm{d}K \qquad \text{and} \qquad C_2(r) = \int_0^\infty S(K)J_2(rK)\Delta(K)\mathrm{d}K. \tag{8}$$

Here, $C_0(r)$ is the isotropic part, whereas $C_2(r)$ denotes the anisotropic part. J_n is the nth-order Bessel function of the first kind. *Figure 2 shows the variations of the isotropic part* $C_0(r)$, the anisotropic part $C_2(r)$ and the full correlation function $C(r, \phi)$ for $\phi = 0$. This function possess a significant negative part that can be a key dependence parameter in some particular scattering cases [27].

In this context, it must be noted that by using equation (7) in (3), the last equation acquires an analytical simplification [26, 16] when the angular integration is evaluated analytically with the help of Bessel functions. However, in this study this simplification is not introduced.

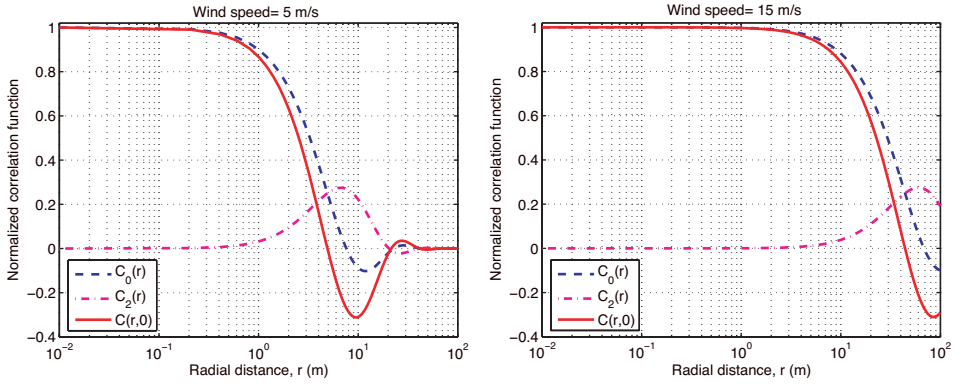

(a) 5 m/s (b) 15 m/s

Figure 2. Variations of the isotropic part $C_0(r)$, anisotopic part $C_2(r)$, and $C(r, 0)$ (upwind case) versus the radial distance at two wind speeds: (a) 5 m/s; (b) 15 m/s.

Indeed, the bistatic normalized radar cross section (NRCS) numerical calculations are made by using equation (3) in a similar way to that used by Voronovich in reference [10] to evaluate the NRCS in the monostatic study (backscattering).

These surface representations will be a key feature when estimating the electromagnetic sea surface scattering object of the next section.

4. Numerical results

In ocean remote sensing applications (wind retrieval, weather forecasting, . . .), the basic idea behind the technique relies on the assumption that the ocean surface normalized radar cross section (NRCS) is strongly correlated with the local surface wind speed and direction. In this section, the normalized radar cross section of the sea surface is studied in bistatic configuration for $F = 14$ GHz (K_u-band) as a function of wind speed, wind direction, scattering angles and polarization states. We use the SSA, model presented in Section 2, and the Elfouhaily model sea surface statistical characteristics, presented in Section 3. We compare the obtained results with those predicted by the two-scale model (TSM) by fixing the K_{d} parameter to $k/3$, where k is the electromagnetic wavenumber. It should be noted that there are many works published for the monostatic case using the SSA model [10, 11, 14–16], but a thorough study has never been done for the fully bistatic configuration, which is our objective here.

4.1 *Forward–backward scattering*

The forward–backward configuration is a particular case of the bistatic configuration where the z-axis, the incident wave vectors and the scattered wave vectors are in the same plane. Figure 3 compares the results yielded by the SSA with those of KA-GO in the forward–backward configuration for two wind speeds: 5 and 15 m/s—cases (a) and (b), respectively. The parameters are fixed as follows: the emitter incident angle is equal to 50°, the emitter azimuth is equal to 0°, the azimuth relative to wind direction is equal to 0 (upwind case), the electromagnetic frequency is fixed at 14 GHz (K_u-band), the receiver azimuth is set to 180° and we vary the receiver incident angle θ_s from −90° to 90°.

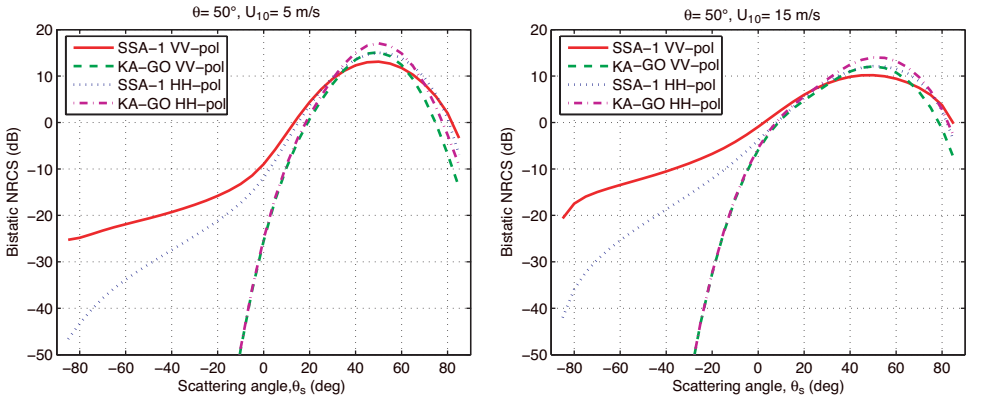

Figure 3. Bistatic diagram in the incidence plane (forward–backward): results with the SSA-1 and the KA-GO models at $\theta = 50^\circ$ and F = 14 GHz for two wind speeds: (a) 5 m/s; (b) 15 m/s.

As is apparent in figure 3, which is the maximum energy is received around the specular direction 50° which is a logical result (because this is the true specular direction as given by Snell's law). This maximum decreases when the wind speed increases. KA-GO works well in the near-specular directions but gives inaccurate results in the directions far from specular, where the Bragg mechanism produces scattering of the same order of magnitude. There is better agreement between the two models in this zone at a wind speed equal to 15 m/s (b) than at 5 m/s (a), but the difference remains within about 2 dB.

4.2 *Fully bistatic configuration*

In this part, we present numerical simulations of scattering cross section from the sea surface by using the SSA model in a fully bistatic configuration as a function of wind speed, incident/scattering angles and polarization states.

It must be noted that we have not found available experimental data in the literature for fully bistatic configurations. Thus, we have chosen to compare the SSA-1 results with those of the well-known theoretical model: TSM.

4.2.1 Scattering angle variation. Figures 4 and 5 show the simulations obtained for wind speed equal to 5 and 15 m/s, respectively. The incident angle is fixed to 40° while the scattering angle varies from 0° to 85° where the incident azimuth is set to 0° and the received one to 135°.

This bistatic configuration is slightly different from the backscattering case. In these figures, we can note that the results provided by the SSA and the TSM results present an interesting similarity. On one hand, for VV-polarization, SSA and TSM are in good agreement with a slight difference for small scattering angles of about 1–2 dB, especially in relative wind speed—figure 4(a)—while for HH-polarization, there is a divergence between them near grazing scattering angles (larger than 60°). This difference becomes more important for high wind speeds—see figure 5(a). On the other hand, when cross polarized cases are considered, it appears that there is a good concordance between results predicted for the VH channel,

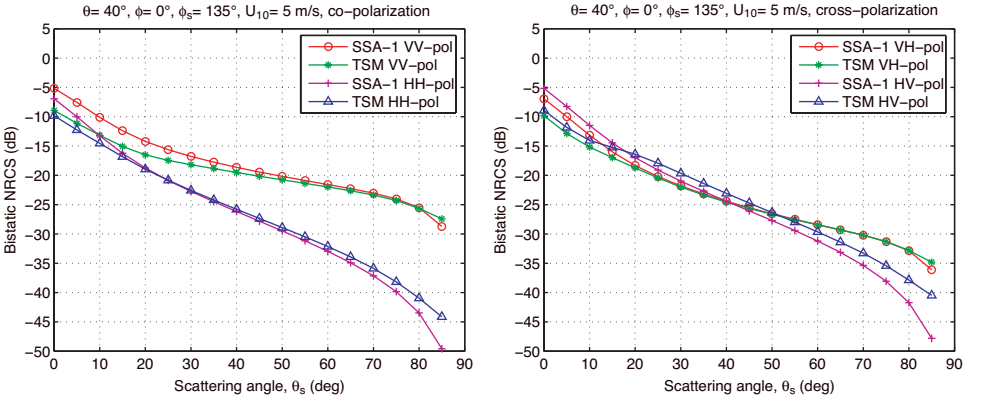

4C/Art

Figure 4. Bistatic scattering cross section with SSA and TSM ($F = 14\,\text{GHz}$, $\theta = 40^\circ$, $\phi = 0^\circ$, $\phi_s = 135^\circ$, wind speed = 5 m/s: (a) co-polarization; (b) cross-polarization).

whereas a disagreement occurs on the HV one especially in the grazing angles zone when the wind speed increases—see figure 5(b).

In order to obtain more relevant information about the behaviour of the SSA in a fully bistatic configuration, we present in figures 6 and 7 predictions at wind speeds equal to 5 and 15 m/s, respectively, with the same parameters as in figures 4 and 5 when the received azimuth is fixed to 45°.

From this bistatic configuration, we can note that the cross-polarization results obtained with the SSA and TSM models in figures 6(b) and 7(b) are in better agreement for large scattering angles than for small ones but there is a little difference near the nadir direction for the VH-polarization. In the co-polarization case, for small scattering angles, the amplitude obtained with SSA is higher than for the TSM one, while for large scattering angles the inverse behaviour takes place. Nevertheless, for HH-polarization the difference between the two models becomes more significant for high wind speed, especially near the grazing

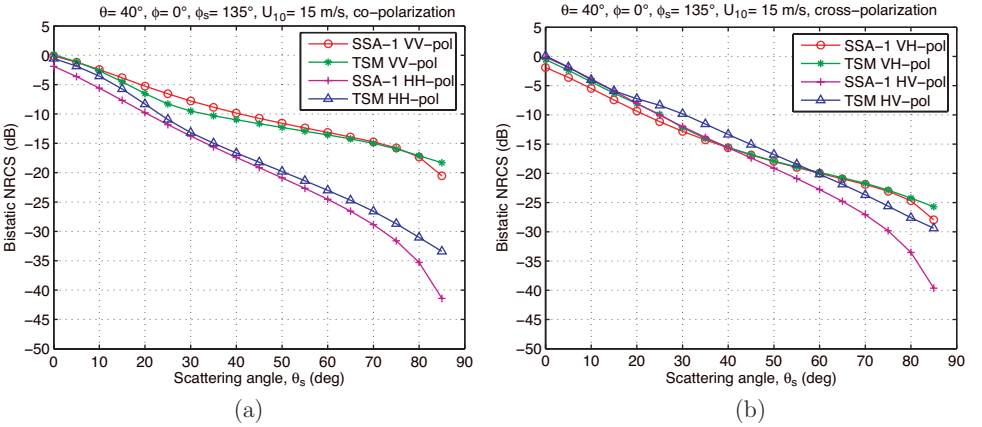

4C/Art

Figure 5. Bistatic scattering cross section with SSA and TSM ($F = 14\,\text{GHz}$, $\theta = 40^\circ$, $\phi = 0^\circ$, $\phi_s = 135^\circ$, wind speed = 15 m/s: (a) co-polarization; (b) cross-polarization).

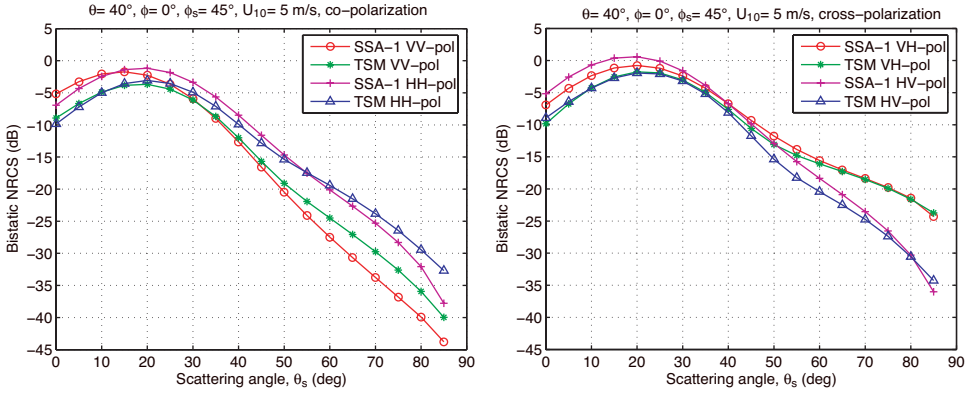

(a) (b)

Figure 6. Bistatic scattering cross section with SSA and TSM ($F = 14\,\text{GHz}$, $\theta = 40^\circ$, $\phi = 0^\circ$, $\phi_s = 45^\circ$, wind speed = 5 m/s: (a) co-polarization; (b) cross-polarization).

angles. One can see that the maximum of the received energy is obtained for scattering angle around 20°. This maximum increases when the wind speed increases, which is a logical result.

4.2.2 Scattering azimuth variation. Figure 8 compares the behaviour of the SSA and the TSM in fully bistatic configurations when the scattering azimuth varies from 0° to 180°. Incident and scattered angles are fixed at 40°, the wind direction is along the x-axis. This evaluation was made for two wind speeds: 5 m/s—case (a)—and 15 m/s—case (b). Varying scattering azimuth angle from 0° to 180°, we obtain several particular configurations. The zero value for the scattering azimuth angle corresponds to forward scattering and an azimuth value of 180° represents backscattering case. For the direction orthogonal to the incident plane, the azimuth angle is equal to 90°. when examining the curves shown in figure 8, several items of importance may be deduced. First, SSA and TSM are in good agreement in both forward- ($\phi_s = 0^\circ$) and back-scattering ($\phi_s = 180^\circ$) configurations, with a small difference

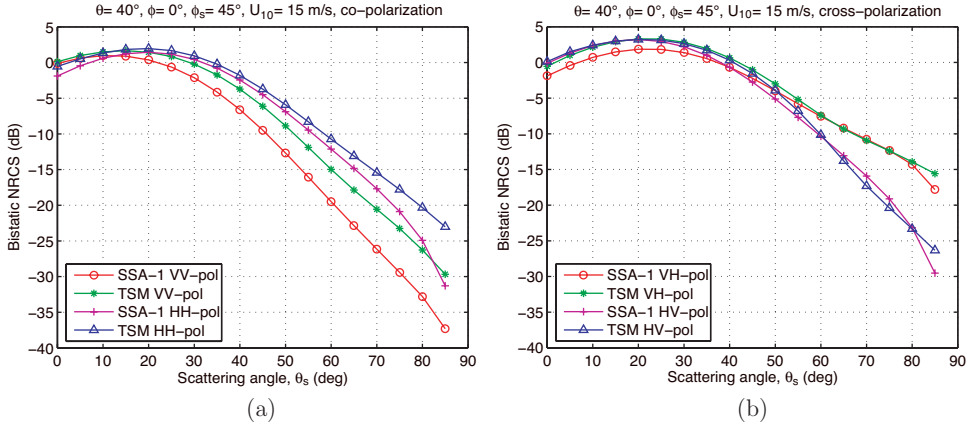

(a) (b)

Figure 7. Bistatic scattering cross section with SSA and TSM ($F = 14\,\text{GHz}$, $\theta = 40^\circ$, $\phi = 0^\circ$, $\phi_s = 45^\circ$, wind speed = 15 m/s: (a) co-polarization; (b) cross-polarization).

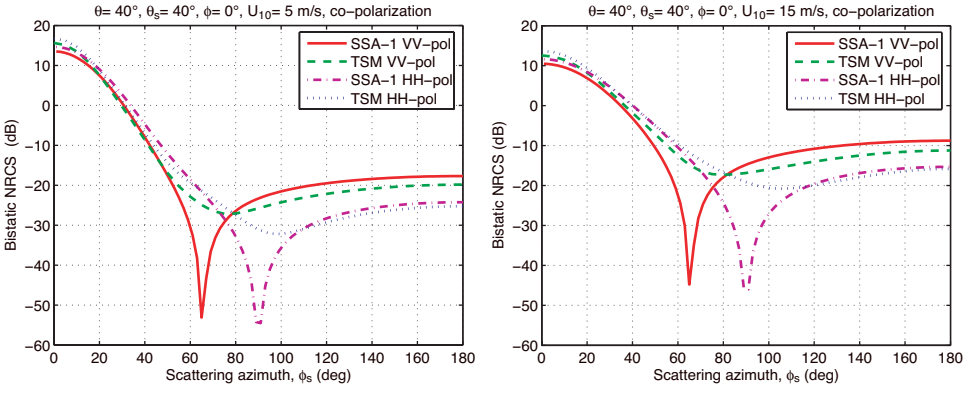

Figure 8. Bistatic scattering cross section with SSA and TSM (F=14 GHz, $\theta = 40^\circ$, $\theta_s = 40^\circ$ $\phi = 0^\circ$, co-polarization coefficients for two wind speeds: (a) 5 m/s; (b) 15 m/s).

that remains within about 1–2 dB. For VV- and HH-polarization, the TSM is weakly below the SSA in the backscattering configuration whereas in forward scattering, the opposite is observed. There is a similarity between SSA and TSM in all scattering planes except in the zone around 50°–70°, where the SSA presents a peak for VV-polarization. For the HH-channel this peak is also present around the plane orthogonal to the incident one (azimuth angle equal to 90°).

The presence of these peaks is not a physical phenomena. The physical and mathematical criteria used in the theoretical development of this model could be the origin of this behaviour. Nevertheless, we are confident that the second order of the SSA model (SSA-2) can remedy this problem, where the numerical computations becomes much more complicated. With the same parameters as in figure 8, cross-polarization results are plotted in figure 9. Note that VH- and HV-polariszation predictions are equal for the SSA model, whereas for the TSM model this is not the case.

As is apparent in figure 9, there is a good agreement between the results obtained with the SSA model and the TSM model in all observed directions except in the forward- and

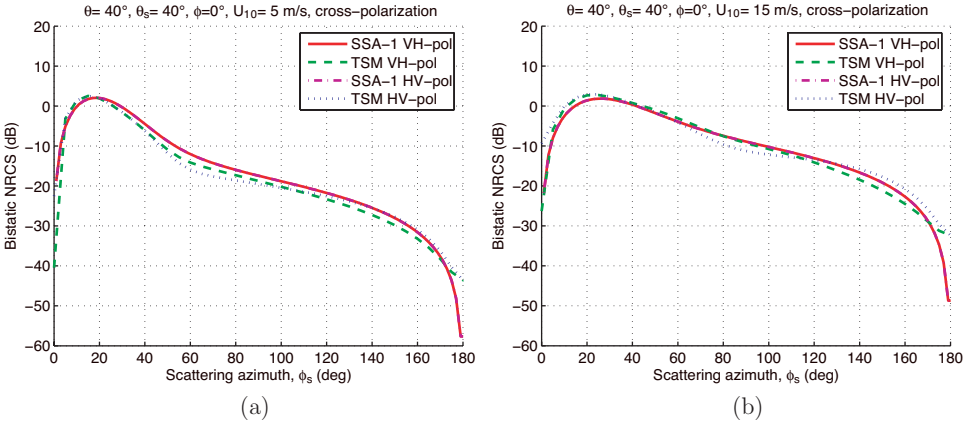

Figure 9. Bistatic scattering cross section with SSA and TSM (F=14 GHz, $\theta = 40^\circ$, $\theta_s = 40^\circ$ $\phi = 0^\circ$, cross-polarization coefficients for two wind speeds: (a) 5 m/s; (b) 15 m/s).

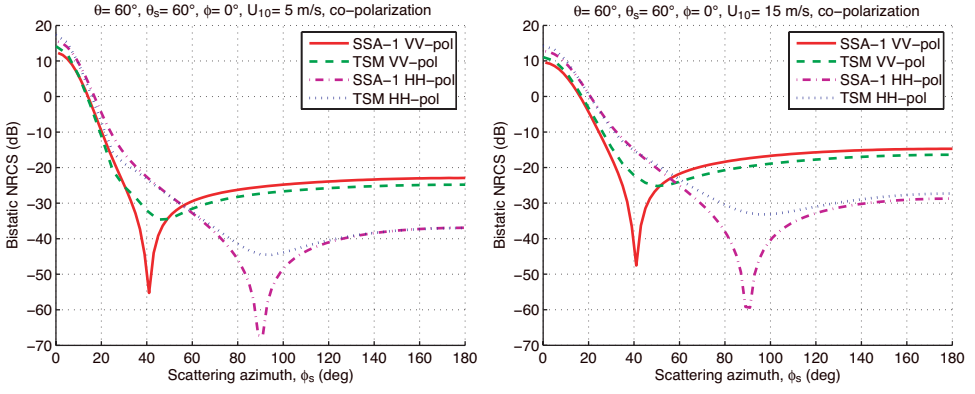

Figure 10. Bistatic scattering cross section with SSA and TSM (F=14 GHz, $\theta = 60^\circ$, $\theta_s = 60^\circ$ $\phi = 0^\circ$, co-polarization coefficients for two wind speeds: (a) 5 m/s; (b) 15 m/s).

the back-scattering configurations. For a wind speed equal to 5m/s (case a), TSM is weakly below SSA where for 15 m/s (case b) there is a better similarity between them. It must be noted that the difference between the two models in the backscattering case becomes more significant with increasing wind speed. In the forward scattering case, the SSA results are clearly above those of the TSM, particularly for relative wind speed—see figure 9(a).

For a deeper analysis, we present in figures 10 and 11 the predictions of the SSA and TSM models with the same parameters as in figures 8 and 9, respectively, but with an incident/scattering angle equal to 60°. Analysing the graphs in these figures, we can confirm the above finding about the behaviour of the SSA model in certain bistatic configurations.

By comparing figures 8 and 10, we can notice that for VV-polarization the position of the peak depends on the value of the incident/scattering angle. Thus, when this value increases the peak moves towards the small azimuth scattering plane. Nevertheless, in the HH case, its position is always in the scattering orthogonal plane ($\phi_s = 90^\circ$).

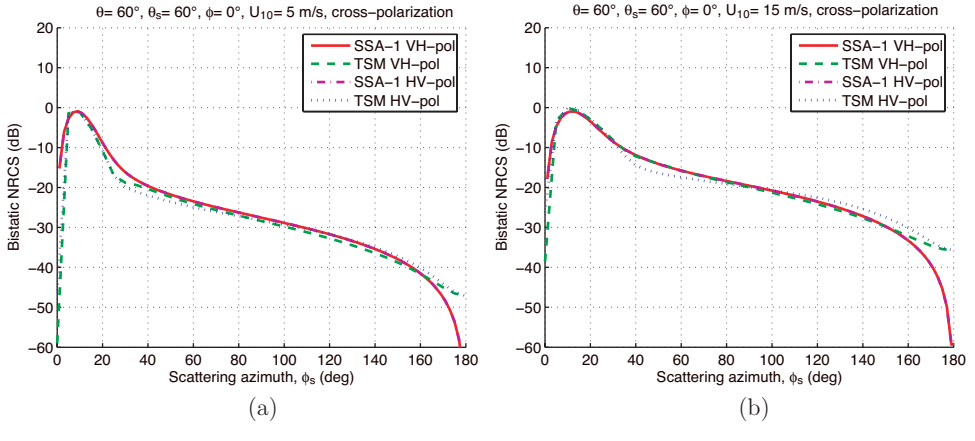

Figure 11. Bistatic scattering cross section with SSA and TSM (F = 14 GHz, $\theta = 60^\circ$, $\theta_s = 60^\circ$ $\phi = 0^\circ$, cross-polarization coefficients for two wind speed (a) 5m/s, (b) 15m/s).

5. Conclusion

SSA-1 has been applied to the numerical prediction of radar sea-surface bistatic scattering cross sections by using the Elfouhaily sea spectrum. The sea roughness was assumed to obey Gaussian statistics and the Elfouhaily sea spectrum was used in numerical calculations. Q2

In the forward–backward case, the results obtained with the SSA-1 model are compared with those predicted by the KA-GO model. There is a good agreement between them near the near-specular direction where it is well known that the KA-GO model works well. Indeed, the difference between them in this zone is less than 2 dB. We can note that the wind direction dependency becomes negligible in forward scattering cases especially for large scattering angles.

Moreover, the results predicted by the SSA-1 model are compared with those of the TSM model in several fully bistatic configuration for co- and cross-polarization. From the numerical examples presented, there is good global similarity and agreement between the two models for bistatic configurations.

On one hand, for co-polarization states, the most important observation in these cases is the presence of a peak in certain bistatic configurations, which is non-physical behaviour. For the VV-polarization, the position of the peak depends on the incidence angle, while for HH this discrepancy is located in the scattering direction orthogonal plane ($\phi_s = 90^\circ$).

On the other hand, for cross-polarization states, a better similarity between the SSA and the TSM results is obtained for all bistatic scattering planes except for forward- and back-scattering, where a remarkable difference is seen. It must be noted that for the SSA model the results obtained with VH-polarization and with HV-polarization are equal, whereas for TSM this is not the case. This study can be considered as an analyse of the behaviour of an anisotropic sea surface NRCS, simultaneously with two scattering models of different categories: the SSA model (unifying category) and TSM (composite one). The simple comparison between these two models can predict the limits of the SSA-1 model in some fully bistatic configurations. We are confident that the second order of the SSA model (SSA-2) can remedy the non-physical phenomena in some fully bistatic configurations, but this has to be established numerical results are obtained by using the SSA model to first order, we suggest introducing the second order in our future work in order to verify if the non-physical phenomena remain. Finally, in this bistatic study, the TSM model presents more coherent results than SSA-1. However, the ultimate verification for the above-obtained results could only be provided by experimental measurements or with benchmark models. This point will be investigated in future work.

Acknowledgements

The authors would like to thank Professor M. Saillard and the unknown referees for their helpful suggestions.

References

[1] Martin-Neira, J., Mavrocordatos, C. and Colzi, E., 1998, Study of a constellation of bistatic radar altimetters for mesoscale ocean applications. *IEEE Transactions on Geoscience and Remote Sensing*, **36**, 1898–1904. Q3

[2] Zavorotny, V. U. and Voronovich, A. V., 2000, Scattering of GPS signals from the ocean with wind remote sensing application. *IEEE Transactions on Geoscience and Remote Sensing*, **38**, 951–964.

[3] Elfouhaily, T. and Guérin, C. A., 2004, A critical survey of approximate scattering wave theories from random rough surfaces. *Waves in Random Media*, **14**, R1–R40.

[4] Rice, S. O., 1963, Reflection of EM from slightly rough surfaces. In: *The Theory of Electromagnetic Waves* (New York: Interscience).

[5] Ogilvy, J. A., 1991, *Theory of Wave Scattering from Random Rough Surfaces* (Bristol: Adam Hilger).
[6] Zavorotny, V. U. and Voronovich, A. V., 1999, Bistatic radar scattering from an ocean surface in the small slope approximation. In: *Proceedings of the IEEE International Geoscience and Remote Sensing Symposium*, pp. 2419–2421.
[7] Fuks, I. M., 1966, Theory of radio wave scattering at a rough sea surface. *Soviet Radiophysics*, **9**, 513–519.
[8] Bass, F. G., Fuks, I. M., Kalmykov, A. I., Ostrovsky, I. E. and Rosenberg, A. D., 1968, Very high frequency radiowave scattering by a disturbed sea surface—Part II: Scattering from an actual sea surface. *IEEE Transactions on Antennas and Propagation*, **AP-16**, 560–568.
[9] Khenchaf, A., 2001, Bistatic scattering and depolarization by randomly rough surfaces: Application to the natural rough surfaces in X-band. *Waves in Random Media*, **11**, 61–89.
[10] Voronovich, A. G. and Zavorotny, V. U., 2001, Theoretical model for scattering of radar signals in K_u- and C-bands from a rough sea surface with breaking waves. *Waves in Random Media*, **11**, 247–269.
[11] McDaniel, S. T., 2001, Small-slope predictions of microwave backscatter from the sea surface. *Waves in Random Media*, **11**, 343–360.
[12] Voronovich, A. G., 1985, Small slope approximation in wave scattering from rough surfaces. *Journal of Experimental and Theoretical Physics*, **62**, 65–70.
[13] Voronovich, A. G., 1994, Small-slope approximation for electromagnetic wave scattering at a rough interface of two dielectric half-spaces. *Waves in Random Media*, **4**, 337–367.
[14] Broschat, S. L. and Thorsos, E. T., 1997, An investigation of the small slope approximation for scattering from rough surfaces—Part II: Numerical studies. *Journal of the Acoustical Society of America*, **101**, 2615–2625.
[15] Bourlier, C. and Berginc, G., 2002, Microwave analytical backscattering models from randomly rough anisotropic sea surface—Comparison with experimental data in C and K_u bands. *in Progress in Electromagnetic Research*, **37**, 31–78.
[16] Bourlier, C., 2004, Azimuthal harmonic coefficients of the microwave backscattering from a non-Gaussian ocean surface with the first-order SSA model. *IEEE Transactions on Geoscience and Remote Sensing*, **42**, 2600–2611.
[17] Gilbert, M. S. and Johnson, J. T., 2003, A study of the higher-order small-slope approximation for scattering from a Gaussian rough surface. *Waves in Random Media*, **13**, 137–149.
[18] McDaniel, S. T., 1999, Acoustic and radar scattering from directional seas. *Waves in Random Media*, **9**, 537–549.
[19] Guérin, C. A. and Saillard, M., 2003, On the high-frequency limit of the second-order small-slope approximation. *Waves in Random Media*, **13**, 75–88.
[20] Elfouhaily, T., Guignard, S., Awadallah, R. and Thompson, D. R., 2003, Local and non-local curvature approximation: A new asymptotic theory for wave scattering, *Waves in Random Media*, **13**, 321–328.
[21] Guérin, C. A., Soriano, G. and Elfouhaily, T., 2004, Weighted curvature approximation: numerical tests for 2D dielectric surfaces. *Waves in Random Media*, **14**, 349–363.
[22] Elfouhaily, T., Chapron, B., Katsaros, K. and Vandemark, D., 1997, A unified directional spectrum for long and short wind-driven waves. *Journal of Geophysical Research*, **102**, 781–796.
[23] Fung, A. K. and Lee, K. K., 1982, A semi-empirical sea-spectrum model for scattering coefficient estimation. *IEEE Journal of Oceanic Engineering*, **7**, 166–176.
[24] Yoshimori, K., Itoh, K. and Ichioka, Y., 1995, Optical characteristics of a wind-roughned water surface: A two dimensional theory. *Applied Optics*, **34**, 6236–6247.
[25] Apel, J. R., 1994, An improved model of the ocean surface wave vector spectrum and its effects on radar backscatter. *Journal of Geophysical Research*, **99**, 16,269–16,291.
[26] Voronovich, A. G., Zavorotny, V. U. and Irisov, V. G., 2000, Sea-roughness spectrum retrieval from radar and radiometric measurements. In: *Proceedings of the IEEE International Geoscience and Remote Sensing Symposium*, Picataway, NJ, pp. 3102–3104.
[27] Awada, A., Khenchaf, A. and Coatanhay, A., 2006, Bistatic radar scattering from an ocean surface at L-band. In: *Proceedings of the IEEE International Radar Conference*, April.

Queries

Q1. Au: Pls. provide dates.
Q2. Au: Please check the wording of this paragraph. The use of commenting-out %-signs in the source file was ambiguous.
Q3. Au: Please titles should be spelled out in full. Please check that the correct full titles have been substituted throughout the references list.